Available online at www.sciencedirect.com
SCIENCE DIRECT®
Journal of Solid State Chemistry 178 (2005) 1807–1817
JOURNAL OF SOLID STATE CHEMISTRY
www.elsevier.com/locate/jssc

Ternary and quaternary layered nitride halides, $Ca_2N(X,X')$ ($X,X' = Cl, Br, I$): Evolution of structure with composition

Amy Bowman[a,1], Ronald I. Smith[b], Duncan H. Gregory[a,*]

[a]*School of Chemistry, University of Nottingham, University Park, Nottingham NG7 2RD, UK*
[b]*ISIS Facility, Rutherford Appleton Laboratory, Chilton, Didcot OX11 0QX, UK*

Received 3 February 2005; received in revised form 7 March 2005; accepted 10 March 2005
Available online 19 April 2005

Abstract

The quaternary systems Ca–N–Cl–Br and Ca–N–Br–I have been investigated resulting in the synthesis of a number of new layered nitride mixed halides. The evolution of structure with composition has been investigated by powder X-ray and powder neutron diffraction techniques. A continuous solid solution exists between Ca_2NCl and Ca_2NBr with intermediate compounds adopting the same *anti*- α-$NaFeO_2$ structure (rhombohedral space group $R\bar{3}m$) as the ternary end members. A phase transition occurs in the $Ca_2NBr_{1-y}I_y$ system between $y = 0.7$ and $y = 0.8$ corresponding to a switch from cubic close packing to hexagonal close packing of metal–nitrogen layers and corresponding adoption of the *anti*-β-$RbScO_2$ (filled *anti*-CdI_2) structure (hexagonal space group $P6_3/mmc$). While nitride and halide anions occupy distinct crystallographic sites, there is no ordering of halides in quaternary materials irrespective of stoichiometry or structure type. All the nitride halides show temperature independent paramagnetic behaviour between 2 and 300 K.

Keywords: Synthesis; Powder X-ray diffraction; Powder neutron diffraction; Structure; Nitrides; Halides; Calcium

1. Introduction

The chemistry of inorganic nitrides has advanced dramatically over the last decade. Among the many binary and higher nitrides formed by the main group and transition elements, it is perhaps curious that many of the most interesting and unusual compounds are formed by the alkali and alkaline earth elements [1,2]. Group 2 metals (A) form nitrides with A–N bonding and structures that change dramatically as one descends the group; the lighter metals (Be–Ca) form ionic, insulating or semiconducting, salt-like compounds whereas the heavier members of the group (Ca–Ba) form subnitrides with low-dimensional structures and metallic properties. The layered subnitrides A_2N (A = Ca–Ba) also provide a structural basis for inclusion of anions from simple spherical species such as halides to more complex, anisotropic entities such as N_2^{2-} and CN_2^{2-} [3,4]. The simplest of the families of "filled subnitrides" are the nitride halides A_2NX (X = F–I) which were originally synthesised several decades ago [5–10]. Only recently, however, have the structures and properties of some of these mixed-anion compounds been scrutinised in more depth [11–15]. Recent work has suggested that the ternary A–N–X phase systems are more complex than originally envisaged and that the structures and anion distributions are sensitive to both the halide (X) and the conditions of synthesis [13–15]. Moreover, variation in structure and anion distribution is likely to have profound effects on electronic properties. For example, in the Mg–N–F system alone, one moves from insulating MgF_2 (calculated direct band gap, E_g, of

*Corresponding author. Fax: +44 115 951 3563.
E-mail address: Duncan.Gregory@Nottingham.ac.uk (D.H. Gregory).
[1]Current address: Department of Chemistry, University of Liverpool, Crown Street, Liverpool, L69 7ZD, UK.

0022-4596/$ - see front matter © 2005 Elsevier Inc. All rights reserved.
doi:10.1016/j.jssc.2005.03.021

6.8 eV) through Mg_3NF_3 ($E_g = 3.6$ eV) and L–Mg_2NF ($E_g = 2.1$ eV) to semiconducting Mg_3N_2 with a direct band gap of 1.6 eV (2.8 eV experimentally [16]).

In a previous communication, we presented results of our preliminary investigations of the quaternary A–N–X–X' (A = Ca, Sr; X,X' = Cl–I) systems and the discovery of the first nitride mixed halides [17]. In this paper we extend our investigations over the entire range of composition in the Ca_2NCl_{1-x}.

Br_x and $Ca_2NBr_{1-x}I_x$ systems from $0 \leqslant x \leqslant 1$ for the first time with the purpose of following the changes in structure and anion distribution in calcium nitride halides with stoichiometry and temperature. Powder neutron diffraction data has provided definitive structural models for the ternary nitride halides Ca_2NCl, Ca_2NBr and Ca_2NI and for key quaternary compounds in the respective Ca–N–Cl–Br and Ca–N–Br–I phase systems. The variations in structure and bonding in the nitride halides are discussed and we set these within the wider context of the growing family of known Ca_2NX mixed anion compounds.

2. Experimental details

2.1. Starting materials

All manipulations were performed in an Ar- or N_2-filled glove box. Calcium nitride Ca_3N_2 was synthesised by the direct reaction of cleaned Ca metal (ca. 8 g cut from an ingot; Alfa, 99 + %) with dried nitrogen at 993 K. The metal was contained in a stainless steel crucible and heated under N_2 (ca. 2 atm) within a closed steel vessel for 24 h. The resulting red block was obtained after cooling and the identity of the ground nitride powder was confirmed by powder X-ray diffraction (PXD) by reference to the ICDD Powder Diffraction File (PDF Card No. 4-854) with negligible alkaline earth oxide impurities in the products.

Binary halides, $CaCl_2$ (Alfa, 99.9%), $CaBr_2$ (Alfa, 99.5%) and CaI_2 (Strem, 98 + %) were obtained commercially. Each was pre-dried by heating in a dynamic vacuum (10^{-4} atm) at 380 K for 14 h. The anhydrous nature and the purity of the halides were verified by PXD.

2.2. Nitride halide synthesis

Ternary and quaternary materials (ca. 0.5 g) were prepared by reaction of Ca_3N_2 with the respective calcium halide(s). All manipulations were performed in a purified Ar-filled glove box. The powders were mixed and ground in overall 1:1 ratios as described in Eq. (1) and pressed as pellets. For X = Cl, X' = Br, x was varied between 0 and 1 in 0.1667 increments. For X = Br, X' = I, x was varied between 0 and 0.6 in 0.2 increments and then in 0.1 increments to $x = 1$. Pellets were wrapped in molybdenum foil and placed within stainless steel crucibles, which were subsequently welded closed under Ar. Crucibles were fired for 5 days at 1393 or 1073 K for (Cl, Br) and (Br,I) samples, respectively, and cooled at 20 K h^{-1} to room temperature. Crucibles were opened in a nitrogen-filled glove box. No reaction of the nitrides with the interior of the Mo foil was observed. Reactions yielded powders of off-white Ca_2NCl, pale yellow Ca_2NBr and yellow Ca_2NI and intermediate compositions $Ca_2NX_{1-x}X'_x$ all of which contained a minor impurity phase of CaO:

$$Ca_3N_2 + (1-x)\ CaX_2 + xCaX'_2 \rightarrow 2Ca_2NX_{1-x}X'_x. \quad (1)$$

Larger samples (ca. 2 g) of selected composition were subsequently prepared by the same method for powder neutron diffraction experiments as detailed below.

2.3. Characterisation by PXD and scanning electron microscopy (SEM)

PXD data were collected using a Philips XPERT $\theta-2\theta$ diffractometer with CuK_α radiation or a Bruker D8 Advance diffractometer with Cu$K_{\alpha1}$ radiation. Samples were loaded in a nitrogen-filled glove box and data for air-sensitive materials were collected using custom-designed sealed sample holders [18]. Cell parameters and phase purity were evaluated from 2 h step scans over 5–80° 2θ with step size 0.02° 2θ using DICVOL91 [19] for indexing and Philips IDENTIFY and Bruker EVA routines for phase identifcation. Lattice parameters were refined by least squares fitting of PXD data. Reflections for ternary and quaternary phases could be assigned to either space group $R\bar{3}m$ or $P6_3/mmc$ depending on halide composition as described below and patterns matched well to those calculated by POWDERCELL 2.3 [20] from previous single crystal data for Ca_2NCl(Br) and Ca_2NI [11,12]. Refined cell parameters for the powders of the ternary phases were in excellent agreement with those reported originally for single crystals of the respective nitride halides.

Morphology of microcrystalline products was investigated by SEM using a Phillips XL 30 ESEM-FEG instrument running at 10.0–20.0 kV under nitrogen. Elemental analysis was simultaneously performed by energy dispersive analysis of X-rays (EDX), taking area and point scans of samples. The air-sensitive samples were loaded into the SEM under a stream of N_2 gas.

2.4. Structure determination from powder neutron diffraction

Time of flight (TOF) PND data were collected for ca. 2 g samples of Ca_2NCl (**1**), Ca_2NBr (**2**), Ca_2NI (**3**) and

the quaternary compounds of nominal composition $Ca_2NCl_{0.5}Br_{0.5}$ (**4**) and $Ca_2NBr_{0.25}I_{0.75}$ (**5**) using the high-intensity diffractometer POLARIS at the ISIS spallation source, Rutherford Appleton Laboratory. Data for all compounds were collected at 293 K. Data were also collected for the mixed chloride bromide (**4**) at 150 and 75 K to investigate possible anion ordering at reduced temperature. Diffraction data were collected using the ^{3}He tube low angle and backscattering detector banks at $\langle 2\theta \rangle = 35^\circ$ and $\langle 2\theta \rangle = 145^\circ$ and the ZnS scintillator detector bank at $\langle 2\theta \rangle = 90^\circ$. Samples were contained in 6 mm diameter, thin walled, cylindrical vanadium sample cans. The cans were loaded in a nitrogen-filled glove box and sealed with indium gaskets. The structures of the nitride halides were refined following the Rietveld method using the General Structure Analysis System (GSAS) software through the EXPGUI interface [21,22]. Initial models were taken from single crystal X-ray data [11,12] and our own indexed PXD data. A convolution of back-to-back exponentials with a pseudo-Voigt function (peakshape function 3 within GSAS) was used to model peak shapes and the background in each case was modelled by an exponential expansion function (background function 6 within GSAS), with up to 6 refined coefficients, accounting for contributions at both low and high Q. Initial cycles allowed for the variation of the scale factor, background and lattice parameters. As the refinements progressed atomic positions, peak width parameters, profile coefficients, isotropic temperature factors and, for quaternary phases, halide site occupancy was introduced. Anisotropic temperature factors were refined for each site in final cycles without any loss of refinement stability. CaO was simultaneously refined as an impurity phase in the profile for each sample (yielding wt% values of: 17.5(1) for **1**, 9.6(1) for **2**, 4.7(1) for **3**, 7.2(1) for **4**, 4.7(1) for **5**). $CaCl_2$ was also included as a third phase in the Ca_2NCl refinement (3.4(2) wt%). In each case, the crystal structure was refined using data collected from all three detector banks simultaneously.

2.5. Property measurements

Variable temperature magnetic susceptibility measurements were performed on samples of the ternary materials, **1**, **2** and **3** (ca. 90 mg) using a Quantum Design MPMS-XL 5 T SQUID magnetometer. All samples were loaded in a nitrogen-filled recirculating glove box. Data were collected between 5 and 250 K under fields of 10^3 or 10^4 Oe with points at 1 K intervals between 5–30 and 5 K intervals from 30 to 250 K. Data were corrected for the diamagnetic contribution of the sample holders (gelatine capsules).

Two point resistivity measurements were performed on pressed pellets of **1**, **2**, and **3** using a Keithley 175A autoranging digital multimeter in a nitrogen-filled recirculating glove box at 293 K. All samples tested, however, gave resistance values above the upper limit of measurement (200 MΩ), strongly supporting the premise that the nitride halides are insulators.

3. Results and discussion

3.1. Characterisation of ternary and quaternary materials

SEM micrographs revealed that representative nitride halide samples (**1**, **2** and **4**) formed plates or irregular blocks between 20 and 50 μm across. Point scans of samples of **1** and **2** yielded Ca:X ratios approximating 2:1 consistent with the expected stoichiometry of the nitride halides. EDX data for samples of **4** gave approximate Ca:Cl:Br ratios of 4:1:1.

PXD patterns of the Ca–N–Cl–Br and Ca–N–Br–I nitride halides are shown in Figs. 1 and 2, respectively. All of the samples contain small amounts of CaO but are otherwise phase-pure by PXD. All compounds in the Ca–N–Cl–Br system could be indexed to the rhombohedral $R\bar{3}m$ cell (isotypic to $Ca_2NCl(Br)$). Within the Ca–N–Br–I system, all compounds with $x \leqslant 0.7$ index in rhombohedral space group $R\bar{3}m$, whereas compounds with $x \geqslant 0.8$ index in space group $P6_3/mmc$ (isotypic to Ca_2NI). Within both systems there is a clear trend of a shift to lower 2θ as the smaller halide anion is progressively replaced by its larger counterpart. This is commensurate with the expected increases in cell volume across the solid solutions. Both the quaternary systems show a steady, approximately linear, increase in both a and c parameters with halide content, x (Fig. 3). The expansion in both systems is anisotropic and more pronounced along c than a (e.g. 4.3% expansion along c vs. 1.4% along a from Ca_2NCl to Ca_2NBr). The

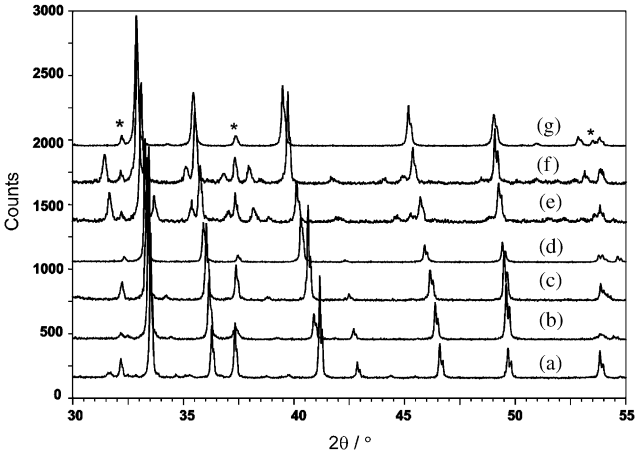

Fig. 1. PXD patterns of $Ca_2NCl_{1-x}Br_x$ nitride halides for $0 \leqslant x \leqslant 1$. Calcium oxide (CaO) peaks are denoted by the asterisk. Patterns shown are for (a) $x = 0$ (Ca_2NCl), (b) $x = 0.167$, (c) $x = 0.333$, (d) $x = 0.5$, (e) $x = 0.667$, (f) $x = 0.833$ and (g) $x = 1$ (Ca_2NBr).

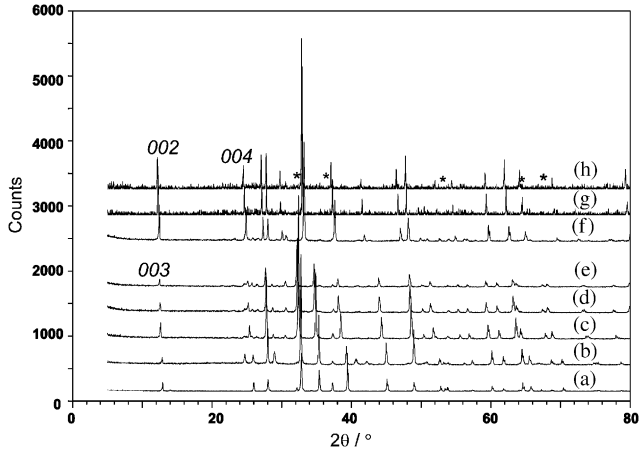

Fig. 2. PXD patterns of $Ca_2NBr_{1-x}I_x$ nitride halides for $0 \leqslant x \leqslant 1$. Calcium oxide (CaO) peaks are denoted by the asterisk. Patterns shown are for (a) $x = 0$ (Ca_2NBr), (b) $x = 0.2$, (c) $x = 0.4$, (d) $x = 0.6$, (e) $x = 0.7$, (f) $x = 0.8$, (g) $x = 0.9$ and (h) $x = 1$ (Ca_2NI). The (003) reflection for the $R\bar{3}m$ phase and the (002) and (004) reflections for the $P6_3/mmc$ phase are indicated.

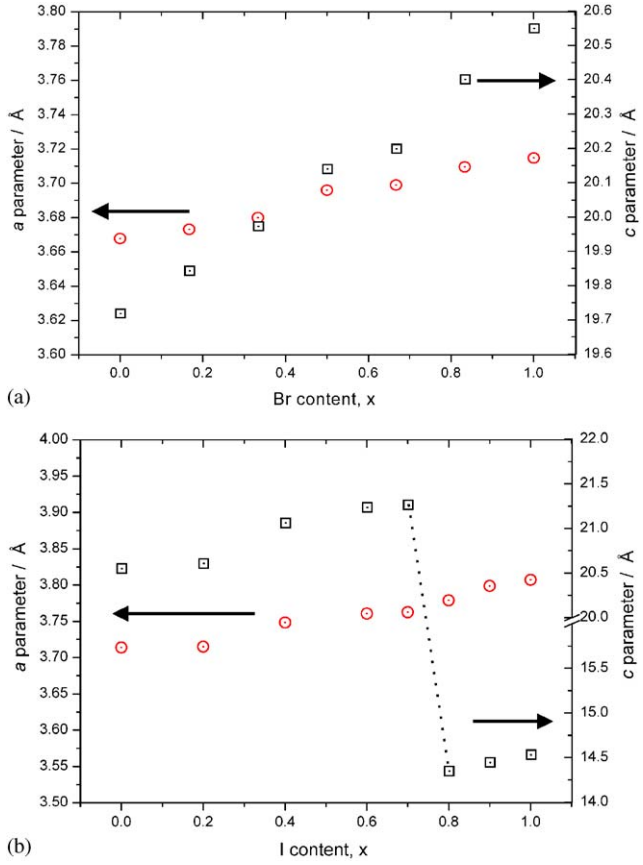

Fig. 3. Plot of variation of unit cell parameters, a (open circles) and c (open squares) against x for (a) $Ca_2NCl_{1-x}Br_x$ and (b) $Ca_2NBr_{1-x}I_x$ nitride halides for $0 \leqslant x \leqslant 1$.

contrast between the 2 quaternary systems lies in the different structures of the end members of the $Ca_2NBr_{1-x}I_x$ ($x = 0$ vs. $x = 1$) solid solution and hence the presence of a composition-dependent phase transition in the bromide iodide system. PXD data show the $R\bar{3}m - P6_3/mmc$ phase transition to occur between $x = 0.7$ and $x = 0.8$ and hence when the $R\bar{3}m$ structure exceeds a critical c/a ratio of ca. 5.65.

3.2. Structure

The crystallographic data and atomic parameters for the nitride halides are shown in Tables 1–4. Fitted neutron diffraction patterns following Rietveld refinement are shown in Fig. 4. Consistent with PXD experiments, Ca_2NCl, Ca_2NBr and $Ca_2NCl_{0.6}Br_{0.4}$ crystallise with the *anti*-α-$NaFeO_2$ structure (Figs. 5a and 6a) whereas $Ca_2NBr_{0.22}I_{0.78}$ and Ca_2NI form *anti*-β-$RbScO_2$ structures (Fig. 5b, 6b). The filled $CdCl_2$-type layered structure of the (Cl,Br) compounds consists of $[NCa_2]^+$ slabs in which N is co-ordinated octahedrally to six Ca atoms. The layers of edge sharing NCa_6 octahedra lie parallel to the *ab* plane stacked along the *z*-direction. The halide anions $(Cl,Br)^-$ occupy the octahedral voids between these positively charged N–Ca layers. This thus creates alternating edge sharing layers of NCa_6 and $(Cl,Br)Ca_6$ octahedra in a cubic close packed arrangement. Similarly, $Ca_2NBr_{0.22}I_{0.78}$ and Ca_2NI also consist of $[NCa_2]^+$ slabs stacked along the *z*-direction, but here the intermediate halides occupy trigonal prismatic holes between hexagonal close packed N–Ca layers in a filled *anti*-CdI_2-type structure.

PND data for **4** and **5** show that the halide anions in the quaternary compounds (Cl^-/Br^- and Br^-/I^-, respectively) are disordered at room temperature, statistically occupying the site between $[NCa_2]^+$ layers (octahedral *3b* (0,0,0) and trigonal prismatic *2a* (0,0,0) sites, respectively), irrespective of structure type. Further, subambient data for **4** demonstrates that there is no ordering of halides above 75 K and hence the α-$NaFeO_2$ structure is retained at 150 and 75 K.

Additional insight into the structural instability driving the composition-dependent α-$NaFeO_2$-type to β-$RbScO_2$-type phase transition in the Ca–N–Br–I system can be gleaned by considering the ratio of the $[NCa_2]^+$ layer thickness, t to the interlayer distance, d (as defined by Bowman et al. [17]). Using our PND data, this t/d ratio varies from 0.65 in Ca_2N [23] through 0.59 in Ca_2NCl, 0.57 in $Ca_2NCl_{0.6}Br_{0.4}$, 0.55 in Ca_2NBr and 0.50 in $Ca_2NBr_{0.78}I_{0.22}$ to 0.49 in Ca_2NI. Given that t is essentially invariant with X across the range of compositions from **1** to **3** (2% decrease), this ratio is largely determined by the increasing average size of the intercalated anion rather than by changes to the relatively rigid Ca–N framework (d increases by 18% from **1** to **3**). This argument is corroborated by an analysis of bond lengths and angles as seen below. It is interesting to compare and contrast the t/d ratios for the $Ca_2N(X,X')$ compounds above with available data

Table 1
Crystallographic data for $Ca_2N(X,X')$ nitride halides at 298 K

Instrument, radiation			POLARIS, neutron		
Formula	Ca_2NCl (**1**)	$Ca_2NCl_{0.6}Br_{0.4}$ (**4**)	Ca_2NBr (**2**)	$Ca_2NBr_{0.22}I_{0.78}$ (**5**)	Ca_2NI (**3**)
M	129.62	149.05	174.08	210.84	221.07
Crystal system	Hexagonal	Hexagonal	Hexagonal	Hexagonal	Hexagonal
Space group	$R\bar{3}m$ (No. 166)	$R\bar{3}m$ (No. 166)	$R\bar{3}m$ (No. 166)	$P6_3/mmc$(No.194)	$P6_3/mmc$(No.194)
Z	3	3	3	2	2
Calculated density, ρ_X(g cm^{-3})	2.813	3.114	3.521	3.879	4.023
Unit cell dimensions:					
a (Å)	3.6665(1)	3.6937(1)	3.7186(1)	3.7963(1)	3.8053(1)
c (Å)	19.7187(2)	20.1780(2)	20.5668(1)	14.4641(1)	14.5527(1)
V (Å^3)	229.57(1)	238.42(1)	246.30(1)	180.526(2)	182.49(1)
Observations, parameters	12645, 57	12847, 59	12011, 55	12034, 52	11202, 57
χ^2	5.89	2.88	2.76	1.34	1.42
R_{wp}	0.029	0.023	0.023	0.026	0.024
R_p	0.057	0.042	0.036	0.051	0.044

Table 2
Crystallographic data for $Ca_2NCl_{0.6}Br_{0.4}$ (**4**) at reduced temperature

Instrument, radiation	POLARIS, neutron	
Formula	$Ca_2NCl_{0.6}Br_{0.4}$	
M	447.2	
Crystal system	Hexagonal	
Space group	$R\bar{3}m$ (No. 166)	
Z	3	
Calculated density, ρ_X(g cm^{-3})	3.100	3.358
Temperature(K)	150	75
Unit cell dimensions		
a (Å)	3.6871(1)	3.6851(1)
c (Å)	20.1295(2)	20.1130(1)
V (Å^3)	236.99(1)	236.54(1)
Observations, parameters	13090, 54	12756, 57
χ^2	3.32	3.60
R_{wp}	0.014	0.014
R_p	0.023	0.024

for the equivalent strontium nitride halides [13,17]. Whereas Sr_2N [24] has $t/d = 0.65$ as is the case for Ca_2N, Sr_2NCl and Sr_2NBr possess larger t/d ratios (0.62 and 0.57, respectively) than the equivalent Ca compounds suggesting the α-$NaFeO_2$-type structure may be stable over a wider field of composition. We are currently investigating structure-composition dependence in the Sr–N–X–X' quaternary phase system to test this hypothesis.

Selected interatomic distances and angles of interest are shown in Table 5. The Ca–N bond lengths for **1–5** are within the range of those in other calcium nitrides and, importantly, in close agreement to the distances found in the binary compound α-Ca_3N_2 (2.451(2)–2.483(1) Å) [25] and the (unfilled) subnitride Ca_2N (2.4426(4) Å) [23]. Moreover, both Ca–N and Ca–X bond lengths are in excellent agreement with the previous single crystal X-ray data for Ca_2NCl, Ca_2NBr and Ca_2NI [11,12]. Ca–N distances in the nitride halides increase slightly with increasing halide anion radius and, for **4**, increase with temperature, as expected. The Ca–X distances show a direct and approximately linear dependence with (average) halide radius across the range of quaternary compounds. From the refined bond angles, it is apparent that the N–Ca–N angle, ϕ (as defined in Ref. [17]), increases with the average size of the halide and hence the $[NCa_2]^+$ layers become increasingly compressed along the c direction to accommodate the anion within the van der Waals gap of the subnitride structure. With the switch from cubic to hexagonal close packing of $[NCa_2]^+$ layers in **5** and **3** and the corresponding change from octahedral CaX_6 geometry to trigonal prismatic geometry, there is a commensurate step increase in ϕ (and sharp decrease in ∠ Ca–X–Ca). Finally, it is worth highlighting that whereas the Ca–Ca distance across the thickness of the $[NCa_2]^+$ layers changes little with X, the other intralayer Ca–Ca distance (in the ab plane) increases more significantly. This trend is again a feature of the increased angular compression of the edge-sharing NCa_6 octahedra with the increasing radius of X^-.

The relation between key structural data (c parameter, Ca–N, Ca–X bond lengths) and anion type, X^-, can be set within the context of the wider family of calcium nitride halides that are now known. The trends are illustrated in Fig. 7, which also includes the unfilled subnitride Ca_2N [23] (where X = vacancy is assumed to be situated at the *3b*, (0,0,0), site) and the nitride hydride Ca_2NH [26] for comparison. All compounds (including cubic Ca_2NH and Ca_2NF [10] and hexagonal Ca_2NI) have been transformed to the $R\bar{3}m$ cell in the figure for clarity. The trends observed in the mixed halide systems

Table 3
Final atomic parameters for $Ca_2N(Cl,Br)$ nitride halides

Data type, instrument		PND, POLARIS				
Compound		Ca_2NCl (**1**)	$Ca_2NCl_{0.6}Br_{0.4}$ (**4**)	$Ca_2NCl_{0.6}Br_{0.4}$ (**4**)	$Ca_2NCl_{0.6}Br_{0.4}$ (**4**)	Ca_2NBr (**2**)
Temperature (K)		298	298	150	75	298
Ca (*6c*) (0, 0, *z*)	*z*	0.2288(1)	0.2272(1)	0.2273(1)	0.2273(1)	0.2258(1)
	$100 \times U_{11} = U_{22}$ (Å^2)	0.879(15)	0.797(8)	0.481(11)	0.341(10)	0.777(8)
	$100 \times U_{33}$ (Å^2)	0.840(26)	1.105(14)	0.849(22)	0.692(20)	0.855(14)
	$100 \times U_{12}$ (Å^2)	0.439(7)	0.398(4)	0.242(6)	0.171(5)	0.388(4)
N (*3a*) $(0, 0, \frac{1}{2})$:	$100 \times U_{11} = U_{22}$ (Å^2)	0.659(14)	0.577(7)	0.382(10)	0.328(9)	0.595(7)
	$100 \times U_{33}$ (Å^2)	0.757(25)	1.013(14)	0.663(22)	0.561(21)	0.728(14)
	$100 \times U_{12}$ (Å^2)	0.330(7)	0.2884(33)	0.191(5)	0.163(5)	0.2971(34)
(*X*,*X*′) (*3b*) (0, 0, 0)	Occupancy (*X*)	1.0	0.580(6)	0.598(9)	0.602(9)	1.0
	$100 \times U_{11} = U_{22}$(Å^2)	1.022(16)	1.108(10)	0.547(14)	0.410(12)	0.912(10)
	$100 \times U_{33}$ (Å^2)	0.985(26)	1.302(18)	1.178(28)	0.952(26)	0.938(18)
	$100 \times U_{12}$ (Å^2)	0.511(8)	0.554(5)	0.274(7)	0.301(6)	0.456(5)

Where $U_{iso} = \frac{4}{3}[a^2U_{11} + b^2U_{22} + c^2U_{33} + ab\ (\cos\gamma)\ U_{12} + ac\ (\cos\beta)\ U_{13} + bc\ (\cos\alpha)\ U_{23}]$.

Table 4
Final atomic parameters for $Ca_2NBr_{1-y}I_y$ ($y > 0$) nitride halides

Data type, Instrument	PND, POLARIS	
Compound	$Ca_2NBr_{0.22}I_{0.78}$ (**5**)	Ca_2NI (**3**)
Ca (*4f*) $(\frac{1}{3}, \frac{2}{3}, z)$		
z	0.4171(1)	0.4175(1)
$100 \times U_{11} = U_{22}$ (Å^2)	0.874(9)	0.91(1)
$100 \times U_{33}$ (Å^2)	0.948(18)	0.85(2)
$100 \times U_{12}$ (Å^2)	0.436(5)	0.45(1)
N (*2a*) $(0, 0, \frac{1}{2})$		
$100 \times U_{11} = U_{22}$ (Å^2)	0.665(8)	0.66(1)
$100 \times U_{33}$ (Å^2)	0.948(13)	0.95(1)
$100 \times U_{12}$ (Å^2)	0.333(4)	0.33(1)
(*X*,*X*′) (*2a*) (0, 0, 0)		
Occupancy (*X*)	0.22(1)	1.0
$100 \times U_{11} = U_{22}$ (Å^2)	0.863(17)	0.77(2)
$100 \times U_{33}$ (Å^2)	1.277(28)	1.13(3)
$100 \times U_{12}$ (Å^2)	0.432(8)	0.38(1)

$U_{iso} = \frac{4}{3}[a^2\ U_{11} + b^2\ U_{22} + c^2\ U_{33} + ab\ (\cos\gamma)\ U_{12} + ac\ (\cos\beta)\ U_{13} + bc\ (\cos\alpha\ )\ U_{23}]$.

discussed here (**1**–**5**) are reproduced in the extended range of $Ca_2N(X,X')$ compounds. The figure highlights an important distinction, however, between the filled and unfilled (X = vacancy) nitrides. Ca_2NF and Ca_2NH both exhibit (equivalent) *c*-parameters (and Ca–*X* distances), which are smaller than in the parent subnitride itself. Hence, the interplay between anion size effects and $[Ca_2N]^+$ interlayer repulsion is exhibited as we increase the size of the anion. Similar effects are observed (as an antithesis) in layered oxides and chalcogenides on intercalating *cations* between (effectively) *negatively charged* layers [27]. In the $Ca_2N(X,X')$ compounds, when X = F, H the repulsion between positively charged layers is reduced (relative to Ca_2N) leading to contraction of *c* whereas when X = Cl or larger, there is an expansion along *c* concomitant with anion size effects. Of course, in reality the X = F, H compounds are cubic (disordered rock salt and 3D-ordered rock salt, respectively, although there is some dispute as to the true structure of Ca_2NH [13] and a tetragonal form of Ca_2NF (L-Ca_2NF) also exists [14]) and so a 2D layered structure containing anions smaller than X = vacancy (□) appears unsustainable. Recent work has suggested that non-stoichiometric nitride hydrides Ca_2NH_y ($0 \leqslant y \leqslant 1$) may exist with either (or both) hexagonal or (and) cubic structures [13]. Effectively these compounds can be described as $Ca_2NH_{1-x}\square_x$ and one might expect an increase in *c* with *x* as one approaches Ca_2N ($x = 1$). That this trend is not obviously observed may signify competing effects of nitrogen non-stoichiometry.

Application of bond valence calculations in nitride systems is of varied value given the significant covalent contribution often associated with bonds between nitrogen and the less electropositive elements.Nevertheless, Brese and O'Keeffe used valence sums extensively and effectively in their original classification of nitride crystal chemistry in 1992 [28]. The library of known nitrides (and nitride structures) is now expanding rapidly and bond valence parameters will no doubt be refined in accord with this. Useful *qualitative* information can still be obtained from this approach. Bond valence sums were calculated using values from Brese and O'Keeffe [29] for a range of $Ca_2N(X,X')$ compounds and are shown in Table 6. Several broad points are worth stating. First, the valence sums of Ca and N are lower than perhaps expected for all the nitrides. Wagner

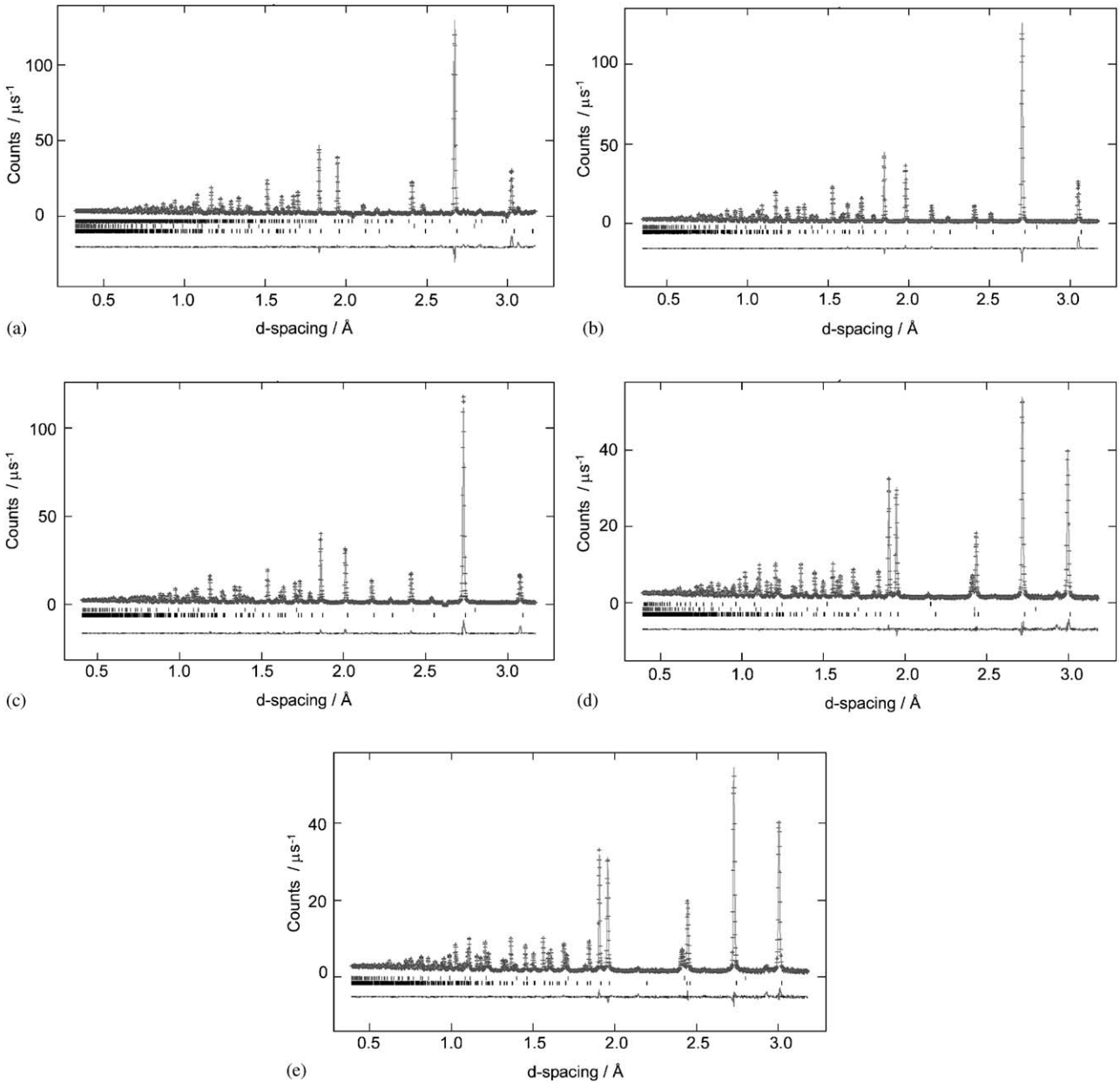

Fig. 4. Observed, calculated and difference (OCD) profile plots for the neutron refinements of (a) Ca_2NCl (**1**), (b) $Ca_2NCl_{0.6}Br_{0.4}$ (**4**), (c) Ca_2NBr (**2**), (d) $Ca_2NBr_{0.22}I_{0.78}$ (**5**) and (e) Ca_2NI (**3**) at 298 K. Crosses depict observed data whereas the solid line depicts the calculated profile. The difference profile is shown below. Tick marks below the profile mark the reflection positions for the $Ca_2N(X,X')$ phases, CaO and, in (a) only, $CaCl_2$. Data collected from the backscattering detector bank ($\langle 2\theta \rangle = 145^\circ$) are shown here.

et al. emphasised this in their bond valence analysis of L-Ca_2NF and discussed the "underbonded" nature of the Ca–N environment [14]. Second, the Ca valence is notably higher (and nearer 2) in the "filled" nitrides vs. Ca_2N. This semi-quantitatively reflects the change in bonding from $[Ca_2N]^+ \bullet e^-$ in Ca_2N to $[Ca_2N]^+(X, X')^-$ in ternary and quaternary compounds. Third, the N valence apparently decreases from $X = Cl$ through $X = Br$ to $X = I$ and as halide electronegativity decreases from 3.0 through 2.8 to 2.5, respectively [30]. DFT calculations show significant covalency in the A–N layers in Sr_2NH, for example (giving an effective charge on N of ca. −1.8) [31]. One would expect the nitride halides to become more covalent with heavier X.

3.3. Properties

Each of the ternary nitride halides display an essentially temperature-independent susceptibility

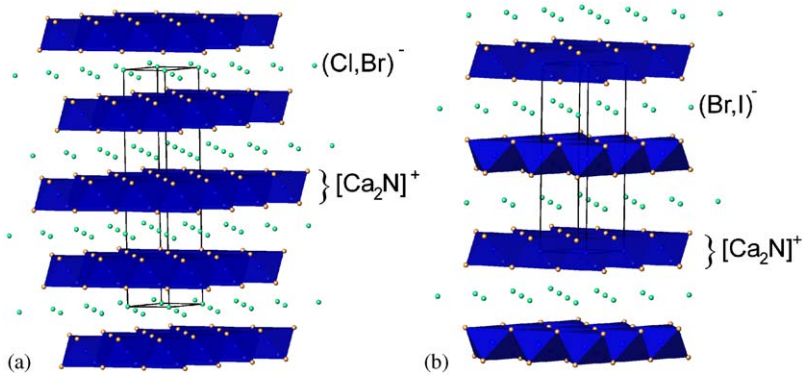

Fig. 5. Crystal structures of (a) $Ca_2N(Cl,Br)$ (*anti*-α-$NaFeO_2$-type) and (b) $Ca_2NBr_{1-x}I_x$ ($x \approx \geqslant 0.75$) (*anti*-β-$RbScO_2$-type). Polyhedra are N-centred NCa_6 octahedra.

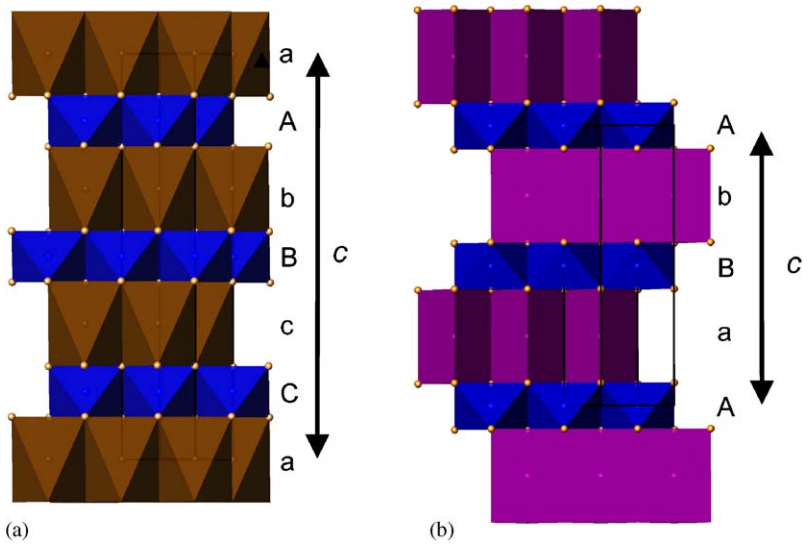

Fig. 6. Crystal structures of (a) $Ca_2N(Cl,Br)$ (*anti*-α-$NaFeO_2$-type) and (b) $Ca_2NBr_{1-x}I_x$ ($x \approx \geqslant 0.75$) (*anti*-β-$RbScO_2$-type) as polyhedral representations showing layer stacking arrangements of edge-sharing NCa_6 octahedra (blue) and either XCa_6 octahedra (brown) or trigonal prisms (purple).

Table 5
Selected interatomic distances and angles for $Ca_2N(X,X')$ nitride halides

Compound	Ca_2NCl (**1**)	$Ca_2NCl_{0.6}Br_{0.4}$ (**4**)	$Ca_2NCl_{0.6}Br_{0.4}$ (**4**)	$Ca_2NCl_{0.6}Br_{0.4}$ (**4**)	Ca_2NBr (**2**)	$Ca_2NBr_{0.22}I_{0.78}$ (**5**)	Ca_2NI (**3**)
Temperature (K)	298	298	150	75	298	298	298
3 × Ca–Ca (Å)	3.2390(7)	3.2421(4)	3.2378(7)	3.2376(7)	3.2455(4)	3.2490(7)	3.2539(7)
6 × Ca–Ca (Å)	3.6665(1)	3.6937(1)	3.6871(1)	3.6851(1)	3.7187(1)	3.7963(1)	3.8053(1)
3 × Ca–N (Å)	2.4462(2)	2.4574(2)	2.4535(2)	2.4527(2)	2.4679(1)	2.4984(2)	2.5035(2)
3 × Ca–X (Å)	2.9542(3)	3.0226(2)	3.0150(3)	3.0119(3)	3.0818(2)	3.2627(4)	3.2820(4)
Ca–N–Ca (deg)	97.085(12)	97.451(8)	97.423(12)	97.397(12)	97.774(7)	98.884(12)	98.928(13)
Ca–*X*–Ca (deg)	76.713(9)	75.327(6)	75.390(10)	75.431(9)	74.217(5)	71.152(9)	70.862(9)

profile (Fig. 8). Between 20 and 250 K weak paramagnetism is observed with corrected values of $\chi_M \sim 1 \times 10^{-3}$ emu mol^{-1} across the temperature -independent region in all samples. The magnitude and temperature dependence of the molar susceptibility is very similar to that of the "unfilled" subnitrides [23,24]. Evidence of a slight Curie tail is observed below 20 K. This is likely attributable to low concentrations of transition metal

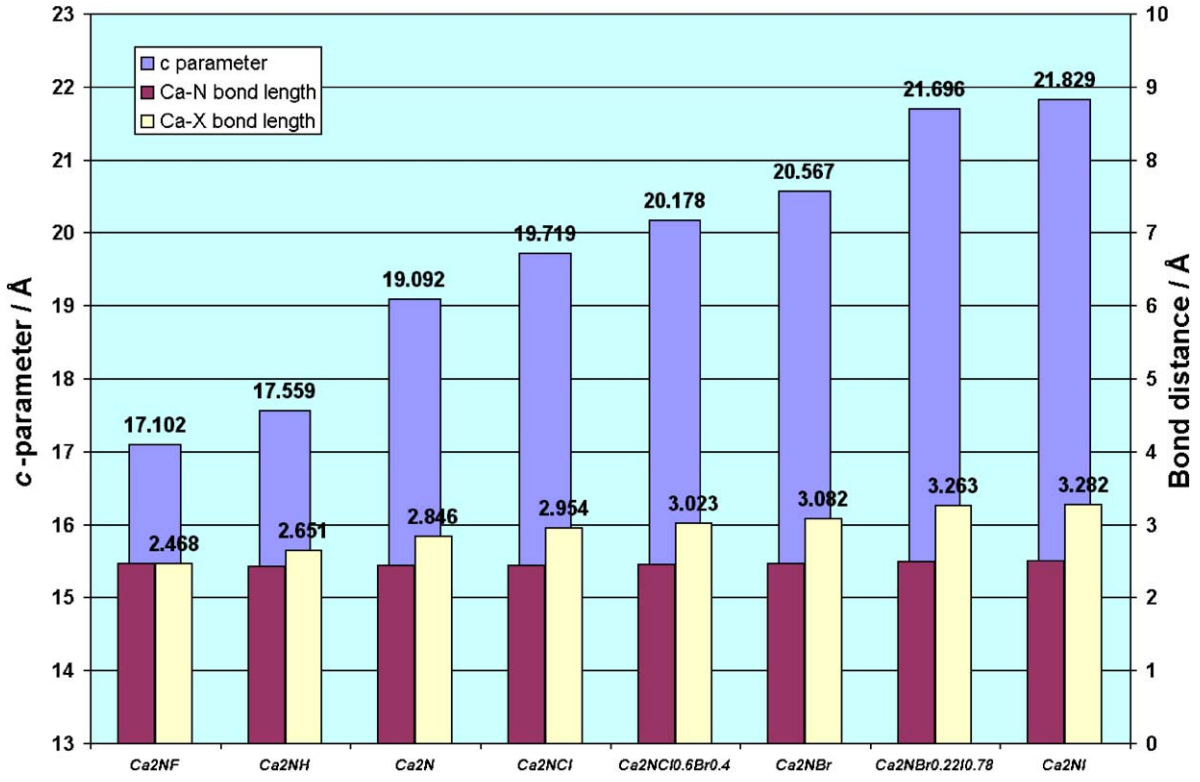

Fig. 7. Histogram plot depicting variation in cell parameters and Ca–N and Ca–X bond lengths for selected Ca_2NX nitrides. Note, cubic (Ca_2NH and Ca_2NF) and the *anti*-β-$RbScO_2$-type nitride cell parameters have been transformed to the $R\bar{3}m$ unit cell. Ca_2N, Ca_2NH and Ca_2NF values are taken from Refs. [10,23,26], respectively.

Table 6
Bond valence sums for Ca_2NX nitrides

Compound	A site valence	N site valence	X site valence	Reference
Ca_2NF ($Fm3m$)	1.8	2.5	1.1	[10]
Ca_2NF ($I4_1/amd$)	1.8	2.7	0.9	[14]
Ca_2NH(D)	1.7	2.8	0.7	[26]
Ca_2N	1.3	2.7	—	[23]
Ca_2NCl	1.9	2.6	1.2	This work
$Ca_2NCl_{0.6}Br_{0.4}$	1.9	2.5	1.2	This work
Ca_2NBr	1.8	2.5	1.2	This work
$Ca_2NBr_{0.22}I_{0.78}$	1.7	2.3	1.1	This work
Ca_2NI	1.8	2.3	1.3	This work

impurities and most likely ppm quantities of steel (or respective component nitrides/oxides) from the reaction crucibles. In each case these impurities are below the detection limits of PND, PXD or EDX. The nitride halides are therefore almost certainly intrinsically diamagnetic or weakly paramagnetic consistent with their formulations, appearance and resistivity measurements at room temperature. Experimental investigations of the electronic properties of the nitride hydrides and halides, $A_2N(X,X')$ (A = Mg–Ba) are by no means extensive. Band structure calculations demonstrate that "unfilled" subnitrides Ca_2N and Sr_2N are metallic (a 2D electron gas is confined between $[NCa(Sr)_2]^+$ layers) [32] whereas rhombohedral (α-$NaFeO_2$-type) Sr_2NH, for example, is a semiconductor with a direct band gap of 1.6 eV [30] (although optical measurements suggest an indirect gap of 2.5 eV [33]). L-Mg_2NF (the only nitride halide for which a band structure has been calculated and isostructural with tetragonal Ca_2NF) is also semiconducting and has an indirect gap of 2.1 eV [16]. It would be interesting to relate systematically the electronic properties of the $A_2N(X,X')$ phases to structure, A and $X(X')$ but this is beyond the scope of this present work.

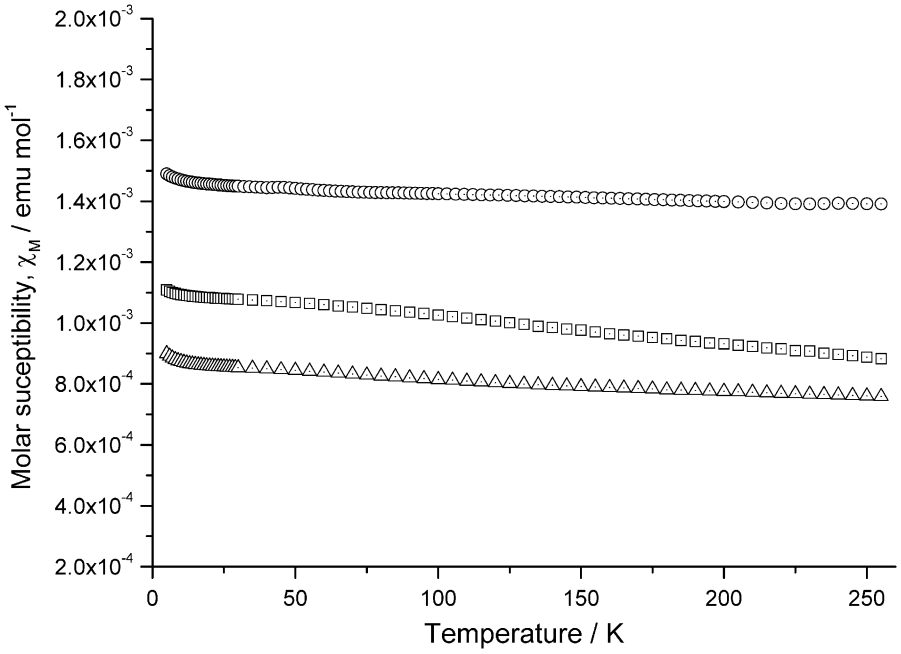

Fig. 8. Plot of molar susceptibility vs. temperature for Ca_2NCl (open squares), Ca_2NBr (open triangles) and Ca_2NI (open circles).

4. Summary

New nitride mixed halides, $Ca_2N(Cl, Br)$ and $Ca_2N(Br, I)$ have been synthesised and structurally characterised by powder X-ray and powder neutron diffraction methods. The nitride chloride bromides form a continuous solid solution between Ca_2NCl and Ca_2NBr and crystallise with the α-$NaFeO_2$ structure. A composition-driven phase transition to the β-$RbScO_2$ structure occurs in the bromide iodide system (between $x = 0.7$ and 0.8 in $Ca_2NBr_{1-x}I_x$). Nitride and halides are ordered in all the ternary and quaternary nitride halides but halides (X,X') remain disordered in the nitride mixed halides irrespective of the halide or of the temperature investigated.

Acknowledgments

We thank the EPSRC for funding this work and the CCLRC for direct access beamtime. We also gratefully acknowledge the University of Nottingham for a studentship for AB.

References

[1] A. Simon, Coord. Chem. Rev. 163 (1997) 253.
[2] D.H. Gregory, Coord. Chem. Rev. 215 (2001) 301.
[3] G. Auffermann, Y. Prots, R. Kniep, Angew. Chem. Int. Ed. 40 (2001) 547.
[4] O. Reckeweg, F.J. DiSalvo, Angew. Chem. Int. Ed. 39 (2000) 412.
[5] P. Ehrlich, W. Deissmann, Angew. Chem. 70 (1958) 656.
[6] P. Ehrlich, W. Deissmann, E. Koch, V. Ullrich, Z. Anorg. Allg. Chem. 328 (1964) 243.
[7] H.-H. Emons, D. Anders, R. Roewer, F. Vogt, Z. Anorg. Allg. Chem. 333 (1964) 99.
[8] H.-H. Emons, W. Grothe, H.-H. Seyfarth, Z. Anorg. Allg. Chem. 363 (1968) 191.
[9] S. Andersson, J. Solid State Chem. 1 (1970) 306.
[10] P. Ehrlich, W. Linz, H.J. Seifert, Naturwissenschaft 4 (1971) 219.
[11] C. Hadenfeldt, H. Herdejürgen, Z. Anorg, Allg. Chem. 545 (1987) 177.
[12] C. Hadenfeldt, H. Herdejürgen, Z. Anorg, Allg. Chem. 558 (1988) 35.
[13] O. Reckeweg, F.J. DiSalvo, Solid State Sci. 4 (2002) 575.
[14] R.A. Nicklow, T.R. Wagner, C.C. Raymond, J. Solid State Chem. 160 (2001) 134.
[15] [a] T.R. Wagner, J. Solid State Chem. 169 (2002) 13;
[b] H. Sebel, T.R. Wagner, J. Solid State Chem. 177 (2004) 2772.
[16] C.M. Fang, K.V. Ramanujachary, H.T. Hintzen, G. de With, J. Alloys Compds. 351 (2003) 72.
[17] A. Bowman, P.V. Mason, D.H. Gregory, Chem. Commun. 351 (2001) 1650.
[18] M.G. Barker, M.J. Begley, P.P. Edwards, D.H. Gregory, S.E. Smith, J. Chem. Soc. Dalton Trans. (1996) 1.
[19] A. Boultif, D. Louer, J. Appl. Crystallogr. 24 (1991) 987.
[20] W. Kraus, G. Nolze, J. Appl. Crystallogr. 29 (1996) 301.
[21] A. C. Larson, R. B. von Dreele, The General Structure Analysis System, Los Alamos National Laboratories, Report LAUR 086-748, LANL, Los Alamos, NM, 2000.
[22] B.H. Toby, J. Appl. Crystallogr. 34 (2001) 210.
[23] D.H. Gregory, A. Bowman, C.F. Baker, D.P. Weston, J. Mater. Chem. 10 (2000) 1635.
[24] N.E. Brese, M. O'Keeffe, J. Solid State Chem. 87 (1990) 134.
[25] O. Reckeweg, F.J. DiSalvo, Z. Anorg, Allg. Chem. 627 (2001) 371.
[26] T. Sichla, H. Jacobs, Eur. J. Solid State Inorg. Chem. 32 (1995) 49.

[27] M.S. Whittingham, A.J. Jacobson (Eds.), Intercalation Chemistry, Academic Press, New York, 1982.
[28] N.E. Brese, M. O'Keeffe, Struct. Bonding (Berlin) 79 (1992) 307.
[29] N.E. Brese, M. O'Keeffe, Acta Crystallogr. B 47 (1991) 192.
[30] L. Pauling, The Nature of the Chemical Bond, third ed., Cornell University Press, New York, 1960.
[31] H. Smolinski, W. Weber, J. Phys. Chem. Solids 59 (1998) 915.
[32] C.M. Fang, G.A. de Wijs, R.A. de Groot, H.T. Hintzen, G. de With, Chem. Mater. 12 (2000) 1847.
[33] Th. Sichla, F. Altorfer, D. Hohlwein, K. Reimann, M. Steube, J. Wrzesinski, H. Jacobs, Z. Anorg. Allg. Chem. 623 (1997) 414.